JOURNAL OF Applied Polymer SCIENCE

Multiwalled Carbon Nanotubes/Polypyrrole/Graphene/Nonwoven Fabric Composites Used as Electrodes of Electrochemical Capacitor

Feifei Liu, Suwen Wang, Gaoyi Han, Ruiqin Liu, Yunzhen Chang, Yaoming Xiao
Institute of Molecular Science, Key Laboratory of Chemical Biology and Molecular Engineering of Education Ministry, Shanxi University, Taiyuan 030006, China
Correspondence to: G. Han (E-mail: han_gaoyis@sxu.edu.cn)

ABSTRACT: The reduced graphene oxide/nonwoven fabric (rGO/NWF) composites have been fabricated through heating the NWF coated with the mixture of GO and $HONH_2 \cdot HCl$ at 130°C, during which the GO is chemically reduced to rGO. Then the composites of polypyrrole (PPy)/rGO/NWF have been prepared through chemically polymerizing pyrrole vapor by using the $FeCl_3 \cdot 6H_2O$ adsorbed on rGO/NWF substrate as oxidant. Finally, multiwalled carbon nanotubes (MWCNTs) are used as conductive enhancer to modify PPy/rGO/NWF through dip-dry process to obtain MWCNTs/PPy/rGO/NWF. The prepared composites have been characterized and their capacitive properties have been evaluated in 1.0*M* KCl electrolyte by using two-electrode symmetric capacitor test. The results reveal that MWCNTs/PPy/rGO/NWF possesses a maximum specific capacitance (C_{sc}) of about 319 F g^{-1} while PPy/rGO/NWF has a C_{sc} of about 277.8 F g^{-1} at the scan rate of 1 mV s^{-1} and that optimum MWCNTs/PPy/rGO/NWF retains 94.5% of initial C_{sc} after 1000 cycles at scan rate of 80 mV s^{-1} which is higher than PPy/rGO/NWF (83.4%). Further analysis reveals that the addition of MWCNTs can increase the charger accumulation at the outer and inner of the composites, which is favorable to improve the stability and the rapid charge-discharge capacity. © 2014 Wiley Periodicals, Inc. J. Appl. Polym. Sci. **2014**, *131*, 41023.

KEYWORDS: carbon nanotubes; composites; conducting polymers; electrochemical capacitors

Received 30 January 2014; accepted 13 May 2014
DOI: 10.1002/app.41023

INTRODUCTION

Energy storage has been considered as a key technology for the development of renewable energy sources and reduction of energy waste. Electrochemical capacitors, used as a kind of energy storage between secondary batteries and traditional capacitors, exhibit an unusually high energy density, long cyclic life and good environmental friendliness.[1–4] Mechanism of energy storage in electrochemcial capactitors predominately includes two ways: the electric double-layer capacitance (EDLC) and pseudocapacitance[5,6] based on the materials of the electrodes.[7,8] Commonly, porous carbon materials are mainly used as the electrodes in EDLC while transition metal oxides and conducting polymers are mainly used in pseudocapacitors.[9] Recently, efforts have been made to improve the rate capability of supercapacitors by designing the microstructures of the materials.

Among the conducting polymers, polypyrrole (PPy) is considered as promising material for electrochemical capacitors[10–12] owing to its high electrical conductivity, high energy storage capacity, low cost, simple synthesis, and the benign property to environment.[13–16] However, the cyclic lifetime of PPy is poor because the repeated ionic exchange in the matrix of polymer during the electrochemical cycles will change the structural conformation of PPy. The combination of PPy and other conductive materials has been considered as effective method to obtain PPy-based electrochemical capacitors with large capacitance, good rate capability, and superior stability, and been attracted a great deal of attentions. Carbon nanotubes (CNTs) exhibit excellent electrical conductivity and high surface area[17–19] and can be utilized as the support for composites or the material of electrode for supercapacitor. Conversely, graphene constructed by one layer of carbon atom is a promising material due to its low cost, remarkable mechanical properties, large surface area, and good electrical conductivity.[20–25] Based on the aforementioned merits, CNTs and graphene have been considered as attractive materials for the PPy-based composites.[10,17,26–30] For example, Sun et al.[31] have got a C_{sc} of about 243 F g^{-1} at a scan rate of 10 mV s^{-1} for the composite of PPy and functionalized multiwalled CNTs (MWCNTs). Electrochemical performance of organometallic functionalized CNTs-based PPy composites, determined by Mi et al.,[32] has achieved a C_{sc} of about 304 F g^{-1} in the low scan rate. Ham et al.[33] have found that the maximum C_{sc} value (in

Additional Supporting Information may be found in the online version of this article.

the presence of binder) for PPy/SWCNTs composite is only about 134 F g^{-1}. Furthermore, PPy/graphene composites have also been investigated by several researchers in order to utilize the composites as a supercapacitor electrode. Biswas et al.[30] have demonstrated a novel architecture involving nanostructured PPy and graphene nanosheets in a multilayered configuration and achieved a C_{sc} value of 164 F g^{-1} with high electrochemical cyclic stability. Furthermore, the composites of PPy/graphene have also been synthesized *in situ* polymerization by Zhang et al.,[10] which indicates that the interaction between PPy and graphene may be probably due to the hydrogen bonding or π-π stacking, and that the nanostructure of PPy is greatly affected by the addition of graphene during the synthesis process.

With the development of the portable wearable electronic devices,[34–36] solar cells,[37] and flexible chemical batteries,[38–40] flexible energy storage devices have stimulated tremendous interest to design new flexible materials for use in capacitors' electrodes. It is well known that the fabrication of new substrates is important because the substrates must meet such requirements as mechanical property, flexibility, and environmentally friendliness in the development of flexible supercapacitor. Till now, the films formed by CNTs and reduced graphene oxide (rGO) have been fabricated and used as conducting substrates to load electroactive materials such as MnO_2, PPy, and polyaniline.[7,10,17,28,41–43] However, the fabrication of films of CNTs and rGO with large area is difficult and costly. Recently, MnO_2 deposited on the flexible substrates coated with CNTs or graphene has been fabricated and it is found that the capacitive properties of MnO_2 have been improved by the addition of the carbon materials.[44,45] It is found in our experiment that the addition of CNTs can improve the capacitive properties of PPy deposited on the substrate of melamine foam[46] which has weak mechanical strength because of its porous structure. However, the contribution of carbon materials for the whole capacitance has not been demonstrated.[44–46] Nonwoven fabrics (NWFs) of polyester, widely used in medicine, clothing, industrial, and agricultural fields, exhibit such advantages as light-weight, high porosity, flexibility, and high elasticity. The NWFs will become ideal substrates for flexible electric devices when the NWFs are coated with conducting material. Recently, graphene has been widely used to fabricate the transparent electrodes and other composites because of its high electrical conductivity. Unfortunately, the rGO prepared from GO has a small solubility in water which is the main limitation for loading more rGO on substrates by using dip-dry method. Owing to the fact that GO can be dispersed in water with high concentration, the mixture of reducer and GO can be loaded on the substrates with large amount by dipping process, then conductive rGO film will be formed on the substrates after being heated at not-high temperature.

In this work, the mixture of GO and reducer (hydroxylamine hydrochloride) is first loaded on the NWFs by dipping process, then the composites are heated at 130°C to obtain the conductive substrates. Consequently, PPy is conveniently deposited on the substrates through a route of vapor polymerization *in situ* according to the literature.[47] To increase the electrical conductivity of the composites further, MWCNTs are loaded on the surface of PPy by dip-dry process. The fabricated composites are characterized and their capacitive properties have been evaluated in detail. Furthermore, the contribution of the additional MWCNTs has also been investigated.

EXPERIMENTAL

Reagents and Materials

Acetonitrile, KCl, $HONH_2{\cdot}HCl$, $FeCl_3{\cdot}6H_2O$, anhydrous ethanol and methanol were of analytical grade and used without further purification. Pyrrole (A.R., Shanghai Chemical Reagent) was purified through distillation under reduced pressure and stored at a temperature less than 5°C. MWCNTs were obtained from department of chemical engineering of Tsinghua University and treated in H_2SO_4-HNO_3 mixed acid.[48] Natural graphite powder (NGP, 325 mesh) was purchased from Tianjin Guangfu Research Institute. The GO was prepared by oxidizing the NGP according to the method reported in literature.[49] NWFs were purchased from Wenjian Medical.

Preparation of the Composites of rGO/NWF

The NWFs were washed by ethanol to remove the impurities before use. Firstly, the GO solution (5.0 mg mL^{-1}) was added into 2.0 mL $HONH_2{\cdot}HCl$ solution (0.125 mol L^{-1}, volume of ethanol : water = 1 : 1), and then the mixtue was treated under ultrasonic condition for 1 min. Secondly, the strips of NWFs (20 × 15 mm) were immersed into the mixture of GO and $HONH_2{\cdot}HCl$ for 5.0 min, then the strips of NWFs were removed from the mixture and transferred to a preheated oven and heated at 130°C for 30 min. During the process, the color of the GO loaded on NWFs changed from brown to black, indicating that the GO was reduced and rGO formed. The composites were named as rGO/NWF and washed by water thoroughly and dried at 130°C.

Preparation of Flexible PPy/rGO/NWF and MWCNTs/PPy/rGO/NWF

The flexible PPy/rGO/NWF was prepared by using $FeCl_3{\cdot}6H_2O$ dissolved in acetonitrile as oxidant to react with the pyrrole vapor in an airtight vessel at room temperature. Briefly, the films of rGO/NWF were soaked in the $FeCl_3{\cdot}6H_2O$ solution of acetonitrile (250 mg mL^{-1}) for 5 min. After the excess solution was eliminated by a filter paper, the rGO/NWF films containing $FeCl_3{\cdot}6H_2O$ solution were suspended in a sealed vessel where the oxidant reacted with the pyrrole vapor at room temperature for 5 h. The composites of PPy/rGO/NWF were dried at 80°C under vaccum for 4 h after the impurity was removed through washing with ethanol and methanol for several times. To improve the conductivity of the composite, the optimum PPy/rGO/NWF composite was immerged in the dispersion of MWCNTs (2 mg mL^{-1}) for 5 min, finally the composite of MWCNTs/PPy/rGO/NWF was obtained after it was taken out and dried at 80°C under vaccum.

Characterization and Electrochemical Measurements

The morphologies of the composites were observed on a scanning electron microscope (JEOL SEM 6701F) and a transmission electron microscopy (TEM, JEOL-2010). The resistances of the composites were measured by using a multimeter (Unitrend Technology, China), the weight of MWCNTs and the PPy in the composites was measured by using a precision balance (Mettler Toledo weighing equipment system). X-ray

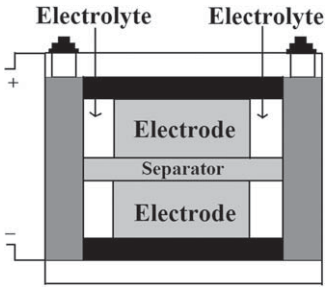

Figure 1. Schematic structure of the capacitors used for test.

photoelectron spectroscopy (XPS) measurements were performed with an AXIS ULTRA DLD spectrometer (Kratos Shimadzu Group company) using a monochromic Al Ka source at 1486.6 eV, the X-ray work power was generally 150 W, and the area of sample ananlysis was about 700 × 300 μm.

The structural illustration of the capacitor cell assembled by the composites was shown in Figure 1. Two nearly identical pieces of (5 × 5 mm) composites were separated by a separator soaked with 1.0 mol L^{-1} KCl aqueous solution after they were immersed into 1.0 mol L^{-1} KCl for 30 min. The capacitors were evaluated by using cyclic voltammetry (CV) and galvanostatic charge/discharge. All the electrochemical performances were measured by using 1.0*M* KCl aqueous solution as electrolyte on a CHI 660C electrochemical station at room temperature. The CV curves of the unit cell were performed within the voltage range of −0.5 to 0.5 V at a scan rate range of 1–200 mV s^{-1}. The C_{sc} of the electrodes was gavanostatically measured at a current density ranging from 0.2 to 10 A g^{-1}. The electrochemical impedance spectra (EIS) were recorded at open-circuit potential in the frequency ranged from 10^5 to 10^{-2} Hz with ac-voltage amplitude of 5 mV.

To analyze the variation of C_{sc} with various scanning rates, the C_{sc} of the electrodes can be calculated based on CV curves according to following equation[50]:

$$C_{sc} = \left(\int IdV\right)/(vm\Delta V) \quad (1)$$

Where I is the response current (A), ΔV the potential difference during the CV tests (V), v the potential scan rate (V s^{-1}), and m the mass of the one electrode (g). Furthermore, the C_{sc} can also be calculated from the galvanostatic charge/discharge curves.[51]

$$C_{sc} = 2(I\Delta t)/(m\Delta V) \quad (2)$$

where I represents the constant discharge current, Δt the discharging time, m the mass of one electrode, and ΔV the voltage drop on discharging.

RESULTS AND DISCUSSIONS

Characterization

To investigate the changes of the element content and the valence before and after GO being reduced, the XPS analyses have been carried out. It is clear that the XPS spectrum of GO shows obvious signals corresponding to O and C element [Figure 2(A-a)]. However, rGO/NWF shows an obvious signals

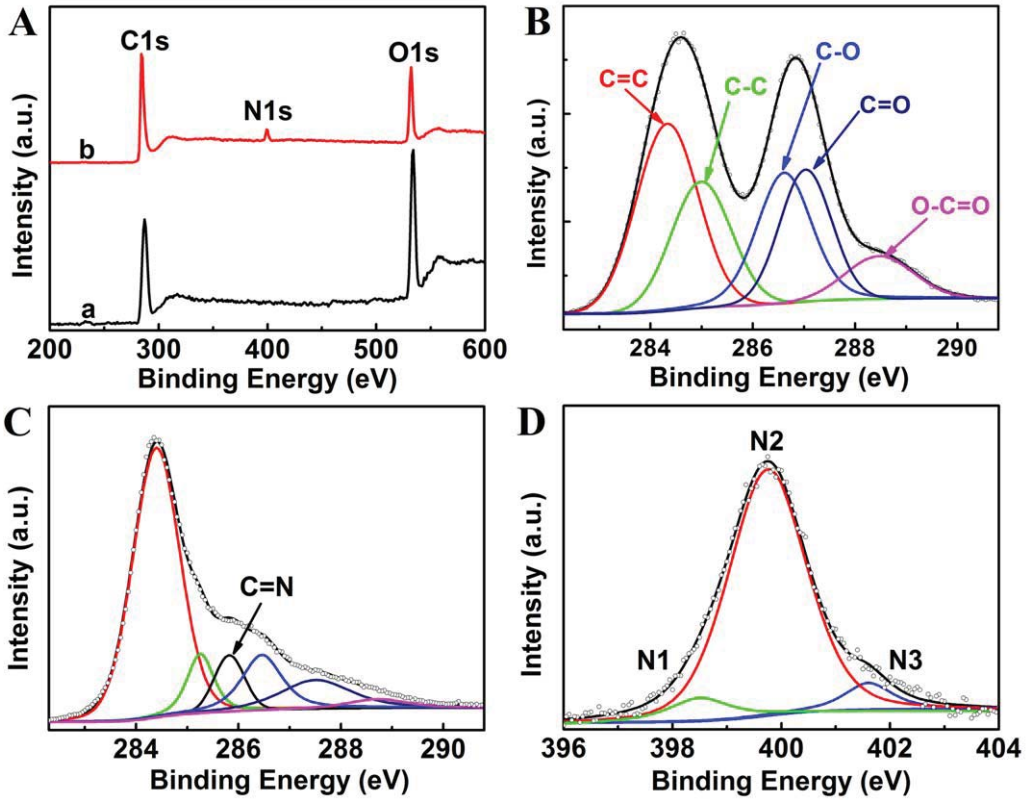

Figure 2. (A) The general XPS spectra of GO (a), rGO (b) and (B) high resolution C1s XPS of GO, (C) rGO, and (D) N1s XPS of rGO. [Color figure can be viewed in the online issue, which is available at wileyonlinelibrary.com.]

Table I. The Atomic Composition of the GO and rGO Measured by XPS

	Elements content (at.%)			Ratios of elements	
Samples	C	O	N	C/O	C/(N + O)
GO	67.3	32.7	0.00	2.06	2.06
rGO	78.93	16.28	4.79	4.85	3.75

of N in the XPS spectrum after the composites have been heated, and the content of C increases and the content of O decreases compared with GO (Table I), which indicates that GO has reacted with hydroxylamine hydrochloride during the heating process [Figure 2(A-b)]. The high-resolution C1s XPS spectrum of GO [Figure 2(B)] can be fitted by the five peaks centered at 284.4, 285.0, 286.6, 28 7.1, and 288.5 eV, which are corresponding to C═C, C─C, C─OR, C═O and O─C═O groups, respectively.[5] However, the intensities of the peaks corresponding to the oxygen-containing groups become weaker after thermally treating [Figure 2(C)], revealing that some of the oxygen-containing groups in GO have been removed during the process of the reaction. The formed C═N bond may be discovered at 285.7 eV. It is noticeable that the peak of C─N is overlaid by C═O and the peak around 286.5 eV can be assigned to C═O and C─N bonds. The N1s XPS peak of the sample shown in Figure 2(D) can be divided into three components: pyridinic-N (N1, 398.4 eV), pyrrolic-N (N2, 399.5 eV), and quaternary-N (N3, 401.6 eV).[52] The analysis based on the data shown in Table I reveals that the C/O ratio increases obviously from 2.06 to 4.85 after the GO has reacted with $HONH_2{\cdot}HCl$. According to the XPS spectra and the data, it is found that the O content in this rGO is relatively high compared with the rGO obtained by hydrothermal method. The electrical conductivity of the composites has been measured by using the two-electrode method and found that the composites of rGO/NFW are almost insulator before being heated, while rGO/NFW exhibits a conductivity of about 0.4 S cm^{-1}.

The SEM image shows that the fibers in NWF are smooth and arranged randomly (Supporting Information Figure S1) and it is interesting to find that the fibers of NWF have been wrapped by rGO sheets closely due to the surfance tension of solvent except that some rGO sheets stand on the surface of fibers [Figure 3(A)]. However, the surface of the fibers becomes rough and the diameter of the fibers changes large slightly in the composite of PPy/NWF after the fibers are coated with PPy [Figure 3(B)]. As depicted in Figure 3(C), it is found that the films formed by PPy particles have covered the surface of the fibers in rGO/NWF, and that the surface of the fibers becomes rougher with the increase of the content of PPy. Furthermore, the rGO sheets become hardly to be seen, which may indicate that the rGO sheets have been coated with PPy [Figure 3(C) inserted figure]. From the SEM of MWCNTs/PPy/rGO/NWF presented in Figure 3(D), it can be found that a thin layer of MWCNTs has been coated on the PPy, which will enhance the conductivity and improve the capacitive performance. The TEM image shown in Figure 3(D) (inserted figure) demonstrates that

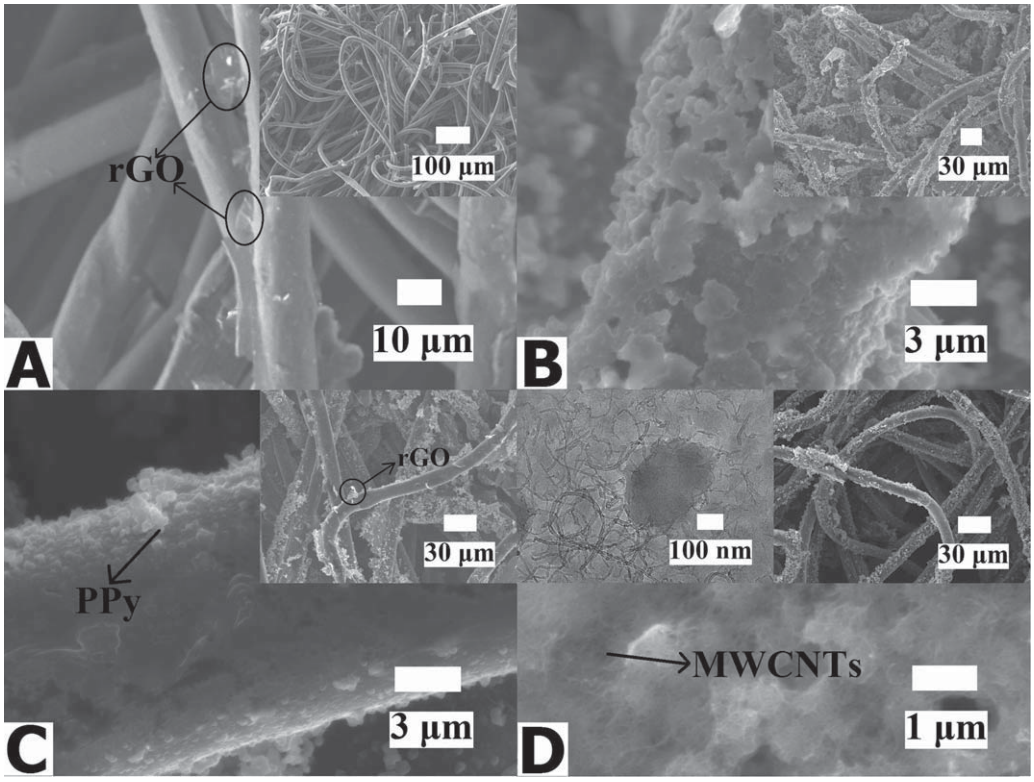

Figure 3. The SEM images of rGO/NWF (A), PPy/NWF (B), PPy/rGO/NWF (C), and MWCNTs/PPy/rGO/NWF (D). The inserted figures are the SEM images in low magnification and TEM image.

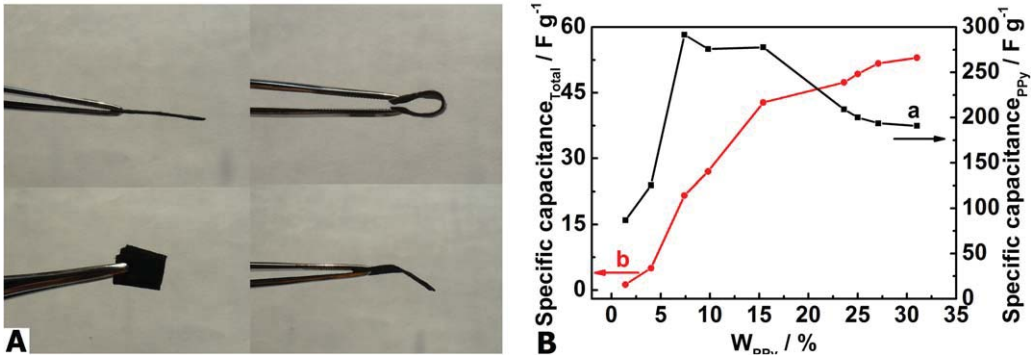

Figure 4. The photograph of the MWCNTs/PPy/rGO/NMF composite under bending condition (A).The relationships between the specific capacitance based on the active material and the total electrode for PPy/rGO/NWF and the content of PPy in the composites (B). [Color figure can be viewed in the online issue, which is available at wileyonlinelibrary.com.]

some particles with large size exhibit in the composites and MWCNTs are dispersed on the surface of PPy/rGO composites.

The Capacitive Properties of the Composites

Figure 4(A) shows the photographs of MWCNTs/PPy/rGO/NMF composite in the bending state, and it can be seen that the composite exhibits good flexibility. The relationship between the C_{sc} and the content of PPy in PPy/rGO/NMF is shown in Figure 4(B), from which it can be seen that the value of C_{sc} based on PPy increases with the increment of PPy in the composites initially and reaches the maximum of 290 F g^{-1}, then maintains almost 277.8 F g^{-1} until the content of PPy reaches to 15.4%. The values of C_{sc} based on PPy decrease slightly when the PPy content is higher than 15.4% and then keep almost constant with the further increase of PPy content. It is well know that the C_{sc} value of PPy is strongly affected by the amount of PPy deposited on substrates. In this case, the composites of rGO/NWF are prepared by dip-dry process, and rGO sheets deposited on the fibers are not more compact, so the composites have less conductivity. Therefore the PPy has small C_{sc} when the PPy content is low because some PPy may be deposited on the insulating fibers of NWF so that some PPy have no contribution to C_{sc}. With the increase of PPy content in the composites, the continuous PPy/rGO films are formed, which makes the C_{sc} of PPy increase because more PPy contribute to the C_{sc}. However, the C_{sc} of PPy will keep constant or decrease with the further increment of PPy's thickness in the composites because the doping/dedoping process of PPy can only easily carry out on the surface. It is interesting that the values of C_{sc} based on the total mass of the composites exhibit a different trend. For example, the value of C_{sc} increases with the increment of PPy, it reaches to about 42.78 F g^{-1} at PPy content of about 15.4% and increases slightly although the content of PPy increases further. So in our experiments, the composite of PPy/rGO/NWF containing 15.4% PPy is chosen as the electrodes of the capacitors in order to make the capacitors have the relatively high capacitance and rapid charge-discharge capacity.

The CV curves of the cells assembled by the composites are recorded between the potential of −0.5 and 0.5 V at different scan rates of 5–200 mV s^{-1} and shown in Figure 5. It can be clearly found that the curves at different scan rates do not show obvious redox peaks in the whole voltage range during both the positive and negative sweeps (Supporting Information Figure S2), indicating that the electrode is charged and discharged at a pseudoconstant rate over the whole CV process. The shapes of the curves are rectangular-like with the almost symmetric I–E responses when the scan rates are lower than 100 mV s^{-1}, which is much better than that of previous report[46] and shows high-rate capacitive properties. It can be also found that the CV curves of MWCNTs/PPy/rGO/NWF [Figure 5(B)] display more rectangular-like than that shown in Figure 5(A), which illustrates that the composite of MWCNTs/PPy/rGO/NWF exhibits better capacitive property than that of PPy/rGO/NWF. Figure 5(C) shows the plots of the variations of C_{sc} versus scan rates ranging from 1 to 200 mV s^{-1}. It can be seen that the values of C_{sc} decrease gradually with the increment of the scan rate for both MWCNTs/PPy/rGO/NWF and PPy/rGO/NWF. Furthermore, it is also found that the composite of MWCNTs/PPy/rGO/NWF exhibits larger C_{sc} at all scan rates and has less decreasing trend than that of PPy/rGO/NWF, which also reveals that MWCNTs covering over PPy can improve the properties of the composites. To clarify the effect of each active material on the C_{sc}, the CV curves of rGO/NWF, PPy/NWF, and MWCNTs/NWF have been measured at different scan rates (Supporting Information Figure S3), and the values of C_{sc} for rGO, PPy and MWCNTs are calculated to be about 118.0, 72.6, and 222.9 F g^{-1} at scan rate of 5 mV s^{-1}, respectively. According to the contents and the C_{sc} values of each component, the total C_{sc} value of the components in composite is calculated to be only about 187.1 F g^{-1} which is far smaller than that of MWCNTs/PPy/rGO/NWF (305.4 F g^{-1}) at the same scan rate, this may indicate that certain synergistic effect exists among these three active materials in the composites. Furthermore, the influence of the amounts of MWCNTs and graphene on the C_{sc} has also been investigated. For example, the decrease of the amounts of graphene and MWCNTs will decrease the C_{sc} value of the composites (Supporting Information Figure S4), which reveals that graphene and MWCNTs in the composites are important because the presence of graphene can increase the surface area of PPy and the MWCNTs loaded on the surface of PPy can enhance the composite's conductivity.

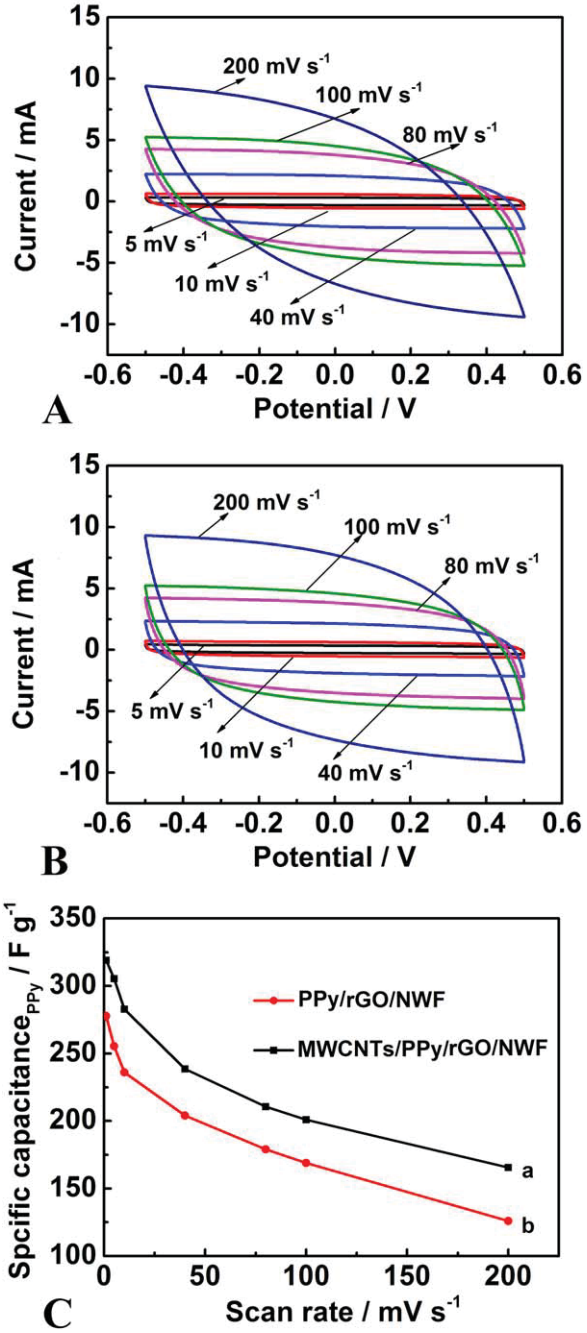

Figure 5. The CV behaviors of the capacitor cells assembled by PPy/rGO/NWF (A) and MWCNTs/PPy/rGO/NWF (B), and the plots of specific capacitances of PPy/rGO/NWF and MWCNTs/PPy/ rGO/NWF versus the scan rates (C). [Color figure can be viewed in the online issue, which is available at wileyonlinelibrary.com.]

Figure 6 shows the typical galvanostatic charge/discharge curves of the cells assembled by PPy/rGO/NWF and MWCNTs/PPy/rGO/NWF at current densities of 0.2, 0.5, 1, 2, and 10 A g^{-1}, it is found that the charging curves are almost symmetric to their discharging counterparts in the whole potential region. It can be also found from Figure 6(A,B) that the *iR* drops increase with the increase of the discharged current densities, and that discharged time is longer and *iR* drop is smaller for MWCNTs/PPy/rGO/NWF compared with PPy/rGO/NWF at the same discharged current density, which indicates that the capacitors of MWCNTs/PPy/rGO/NWF have larger C_{sc} and smaller internal resistance. However, the cells fabricated by composite of MWCNTs/PPy/CNTs/ melamine foam have large *iR* drops although the charge/discharge current density is only 1 A g^{-1}. This demonstrates that CNTs/PPy/rGO/NWF exhibits high-rate capacitive properties compared with CNTs/PPy/CNTs/ melamine foam.[46]

From the plots of C_{sc} versus the discharged current density shown in Figure 7(A), it can be seen that the C_{sc} decreases with the increase of discharge currents for all the cells assembled by the composites, but the cell assembled by MWCNTs/PPy/rGO/NWF shows slighter decrement than that assembled by PPy/rGO/NWF. Figure 7(B) shows the efficiency of charging and discharging (ratio of discharged and charged time) of MWCNTs/PPy/rGO/NWF (a) and PPy/rGO/NWF (b), it is also proved that MWCNTs covering over PPy can improve the properties of the composites.

The repeated galvanostatic charge/discharge curves of the cells assembled by the composites at current density of 2 A g^{-1} are shown in Figure 8, from which it is found that the cells assembled by MWCNTs/PPy/rGO/NWF exhibit less deviation from the cut-off potential and better stability compared with that assembled by PPy/rGO/NWF. Furthermore, the capacitor assembled by MWCNTs/PPy/rGO/NWF displays a much lower *iR* drop at the beginning of the discharge process and a longer discharged time. The *iR* drop is usually caused by the overall internal resistance of the devices. Low internal resistance is of great importance in energy-storing devices as less energy will be wasted to produce unwanted heat during charging/discharging processes. These results indicate that MWCNTs/PPy/rGO/NWF is more suitable for fabricating safe and power-saving supercapacitors compared with PPy/rGO/NWF.

The EIS spectra of the capacitors fabricated by the composites are shown in Figure 9(A). The nearly vertical slope of each plot at the low-frequency region indicates a good capacitor behavior of the cells. The negligible high-frequency resistor-capacitor loop shows a good electrode contact.[53] Equivalent series resistances obtained from the Z'-intercept of the plot [Figure 9(A) inset] show that the capacitor assembled by MWCNTs/PPy/rGO/NWF has a smaller resistance than that by PPy/rGO/NWF. As the service life is a very important factor for the electrode of electrochemical capacitor, the stabilities of the cells assembled by the composites have been evaluated by using CV method at a scan rate of 80 mV s^{-1} [Figure 9(B)]. As can be seen, the value of C_{sc} of PPy/rGO/SNWF decreases 16.6% of the initial capacity after 1000 cycles. However, the capacity loss of the cell assembled by MWCNTs/PPy/rGO/NWF is only 5.5% after 1000 cycles, which illustrates that the material of MWCNTs/PPy/rGO/NWF exhibits good durability and may be developed as a suitable material for electrochemical capacitors applications.

To clarify the difference of charge storage further between the composite of MWCNTs/PPy/rGO/NWF and PPy/rGO/NWF, it is essential to estimate the accumulation of total charge (q^*_{total}) in the electrode materials. It is well known that the total charge

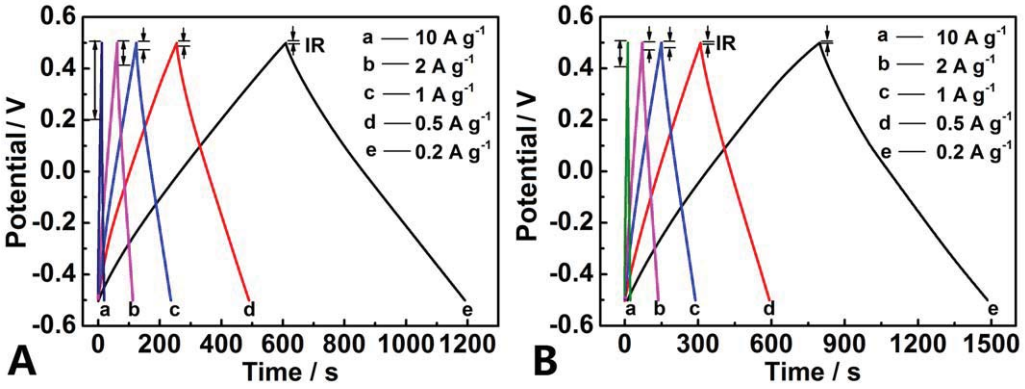

Figure 6. Charged/discharged curves of the cell assembled by PPy/rGO/NWF (A) and MWCNTs/PPy /rGO/NWF (B) at various current densities. [Color figure can be viewed in the online issue, which is available at wileyonlinelibrary.com.]

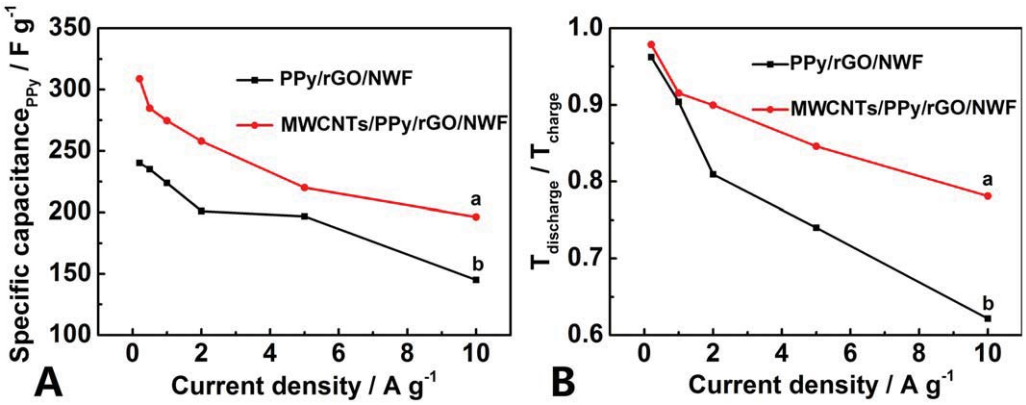

Figure 7. (A) The specific capacitance calculated according to discharge curves of MWCNTs/PPy/rGO/NWF (a) and PPy/rGO/NWF (b) at various discharge current densities, (B) the efficiency of charging and discharging of MWCNTs/PPy/rGO/NWF (a) and PPy/rGO/NWF (b). [Color figure can be viewed in the online issue, which is available at wileyonlinelibrary.com.]

comprises of outer charge (q^*_{out}) coming from the outer region of the materials directly exposed to the electrolyte and the inner charge (q^*_{in}) correlating with the inner part of the materials hidden in pores, grain boundary and so forth. CV is the simplest techniques to evaluate the accumulation of charge. The accumulation of q^* measured by CV at different potential scan rates v (mV s^{-1}) can be usually obtained by integrating the voltammetric curves, and is a mean between the cathodic and anodic branches of CV.[54] Generally, the obtained q^* increases with the decrease of scan rates (v) or with the increase of $v^{-1/2}$. At higher scan rates, the diffusion of ions is limited to the more accessible sites, that is, the outer surface of the materials. Therefore, extrapolation of q^* to the scan rate with $v = \propto$ (i.e., $v^{-1/2} = 0$) from the linear portion of the q^*

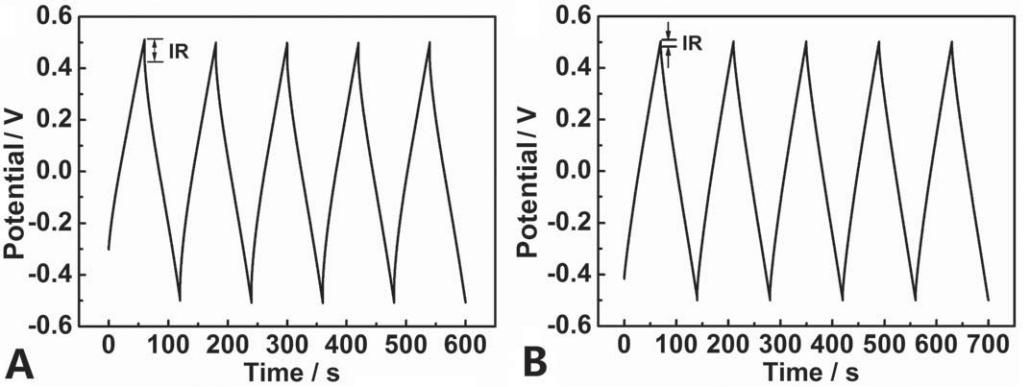

Figure 8. Repeated charged/discharged curves of the cells prepared by PPy/rGO/NWF (A), MWCNTs/PPy/rGO/NWF (B) at current density of 2 A g^{-1}.

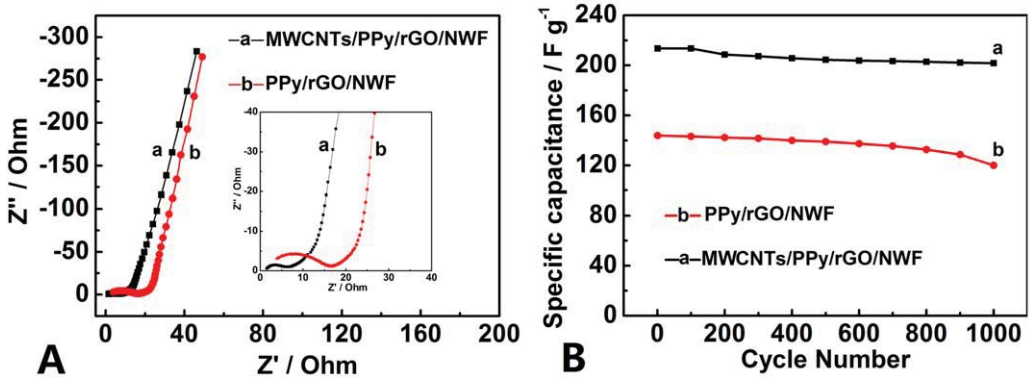

Figure 9. (A) Nyquist plots of the capacitors assembled by PPy/rGO/NWF and MWCNTs/PPy/ rGO/NWF (insert: the high-frequency region). (B) The relationships between the specific capacitance of the cells and the cycle numbers under successive CV scan at 80 mV s^{-1}. [Color figure can be viewed in the online issue, which is available at wileyonlinelibrary.com.]

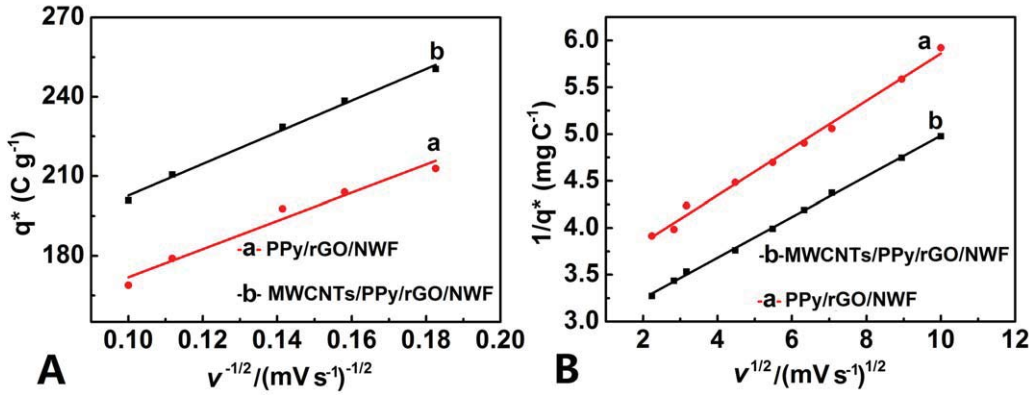

Figure 10. (A) The plots of charge (q^*) determined by voltammetric versus inverse square root of scan rate ($v^{-1/2}$) and (B) the inverse charge ($1/q^*$) versus square root of scan rate ($v^{1/2}$). [Color figure can be viewed in the online issue, which is available at wileyonlinelibrary.com.]

versus $v^{-1/2}$ plot [Figure 10(A)] can provide the accumulation of outer charge q^*_{out} related to the more easily accessible sites. Conversely, total charge q^*_{total} which is related to both inner and outer active sites of the materials can be given from the plot $1/q^*$ versus $v^{1/2}$ by extrapolating [Figure 10(B)] to the scan rate $v = 0$.[55] Then, the charge related to the inner sites needed for higher capacitance can be calculated by the relation of $q^*_{in} = q^*_{total} - q^*_{out}$.

It can be calculated from Figure 10 that the values of $q^*_{total\ (all)}$ on the basis of the active materials are about 301.4 and 351.7 C g^{-1} and the values of $q^*_{out\ (all)}$ are about 118.7 and 141.6 C g^{-1} for the composite of PPy/rGO/NWF and MWCNTs/PPy/rGO/NWF, respectively. Therefore, the values of $q^*_{in\ (all)}$ are calculated to be about 182.7 and 210.1 C g^{-1} for PPy/rGO/NWF and MWCNTs/PPy/rGO/NWF, respectively. Excluding the impact of the MWCNTs (Supporting Information Figure S5), the value of $q^*_{total\ (PPy)}$ is estimated to be about 340 C g^{-1} and the value of $q^*_{out\ (PPy)}$ is calcuated to be about 132 C g^{-1} for MWCNTs/PPy/rGO/NWF, then the value of $q^*_{in\ (PPy)}$ is obtained to be about 208 C g^{-1}. These results reveal that the addition of MWCNTs increases not only the $q^*_{out\ (PPy)}$ but also the $q^*_{in\ (PPy)}$, which makes the MWCNTs/PPy/rGO/NWF own better capacitive properties than PPy/rGO/NWF due to the enhancement of the conductivity caused by MWCNTs.

CONCLUSIONS

The composites of MWCNTs/PPy/rGO/NWF and PPy/rGO/NWF have been synthesized via chemical polymerization of pyrrole monomers in vapor phase. The results of electrochemical measurement reveal that MWCNTs/PPy/rGO/NWF exhibits a relatively larger C_{sc} (about 319 F g^{-1}) than PPy/rGO/NWF (277.8 F g^{-1}) based on the PPy content. The calculated total C_{sc} of the composite based on the C_{sc} values of the components in the composites is much smaller than the fabricated composite of MWCNTs/PPy/rGO/NWF, which indicates that there is synergistic effect among the three active materials in the composites because the presence of graphene can increase the surface area of PPy and the MWCNTs loaded on the surface of PPy can enhance the composite's conductivity. Furthermore, MWCNTs/PPy/rGO/NWF exhibits high rate performance and good cycling stability, for example, the C_{sc} of MWCNTs/PPy/rGO/NWF after 1000 scan cycles can still retain 94.5% of the initial capacitance. The further investigation of the charge storage shows that the presence of MWCNTs can increase not only the accumulation of the outer

charge but also the inner charge, which makes MWCNTs/PPy/rGO/NWF exhibit better performance than PPy/rGO/NWF.

ACKNOWLEDGMENTS

The authors appreciate funding from National Natural Science Foundation of China (21274082 and 21073115) and Shanxi province (2012021021-3), and the Program for New Century Excellent Talents in University (NCET-10–0926).

REFERENCES

1. Stoller, M. D.; Park, S.; Zhu, Y.; An, J.; Ruoff, R. S. *Nano Lett.* **2008**, *8*, 3498.
2. Chang, J. K.; Huang, C.; Tsai, W. T.; Deng, M. J.; Sun, I. W. *J. Power Sources* **2008**, *179*, 435.
3. An, G. M.; Yu, P.; Xiao, M. J.; Liu, Z. M.; Miao, Z. J.; Ding K. L.; Mao, L. Q. *Nanotechnology* **2008**, *19*, 275709.
4. Liu, D. W.; Zhang, Q. F.; Xiao, P.; Garcia, B. B.; Guo, Q.; Champion, R.; Cao, G. Z. *Chem. Mater.* **2008**, *20*, 1376.
5. Chang, Y. Z.; Han, G. Y.; Yuan, J. P.; Fu, D.Y.; Liu, F. F.; Li, S. D. *J. Power Sources* **2013**, *238*, 492.
6. Sahoo, S.; Dhibar, S.; Hatui, G.; Bhattacharya, P.; Das, C. *Polymer* **2013**, *54*, 1033.
7. Liu, J. H.; An, J. W.; Ma, Y. X.; Li, M. L.; Ma, R. B. *Electrochem. Soc.* **2012**, *159*, A828.
8. Yang, G. A.; Xu, C. L.; Li, H. L. *Chem. Commun.* **2008**, *48*, 6537.
9. Conway, B. E.; Pell, W. G. *J. Solid State Electrochem.* **2003**, *7*, 637.
10. Zhang, D. C.; Zhang, X.; Chen, Y.; Yu, P.; Wang, C. G.; Ma, Y. W. *J. Power Sources* **2011**, *196*, 5990.
11. Hepowit, L. R.; Kim, K. M.; Kim, S. H.; Ryu, K. S.; Lee, Y. M.; Ko, J. M. *Polym. Bull.* **2012**, *69*, 873.
12. Norman, L. L.; Badia, A. *J. Am. Chem. Soc.* **2009**, *13*, 2328.
13. Qin, H. Y.; Liu, Z. X.; Yin, W. X.; Zhu, J. K.; Li, Z. P. *J. Power Sources* **2008**, *185*, 909.
14. Han, G. Y.; Shi, G. Q. *Thin Solid Films* **2007**, *515*, 6986.
15. Han, G. Y.; Shi, G. Q. *J. Appl. Polym. Sci.* **2007**, *103*, 1490.
16. Han, G. Y.; Shi, G. Q. *J. Electroanal. Chem.* **2004**, *569*, 169.
17. Lota, G.; Fic, K.; Frackowiak, E. *Energy Environ. Sci.* **2011**, *4*, 1592.
18. Kim, B.; Chung, H.; Kim, W. *J. Phys. Chem. C* **2010**, *114*, 15223.
19. Najafabadi, A. I.; Yasuda, S.; Kobashi, K.; Yamada, T.; Futaba, D. N.; Hatori, H.; Yumura, M.; Iijima, S.; Hata, K. *Adv. Mater.* **2010**, *22*, E235.
20. Kang, Y. R.; Li, Y. L.; Hou, F.; Wen, Y. Y.; Su, D. *Nanoscale* **2012**, *4*, 3248.
21. Zhu, Y. W.; Murali, S.; Cai, W. W.; Li, X. S.; Suk, J. W.; Potts, J. R.; Ruoff, R. S. *Adv. Mater.* **2010**, *22*, 5226.
22. Balandin, A. A.; Ghosh, S.; Bao, W.; Calizo, I.; Teweldebrhan, D.; Miao, F.; Lau, C. *Nano Lett.* **2008**, *3*, 902.
23. Lee, C. G.; Wei, X. D.; Kysar, J. W.; Hone, J. *Science* **2008**, *321*, 385.
24. Becerril, H. A.; Mao, J.; Liu, Z. F.; Stoltenberg, R. M.; Bao, Z. N.; Chen, Y. S. *J. Am. Chem. Soc.* **2008**, *2*, 463.
25. Pradhan, S. K.; Nayak, B. B.; Sahay, S. S.; Mishra, B. K. *Carbon* **2009**, *47*, 2290.
26. Fang, W. C.; Chyan, O.; Sun, C. L.; Wu, C. T.; Chen, C. P.; Chen, K. H.; Chen, L. C.; Huang, J. H. *Electrochem. Commun.* **2007**, *9*, 239.
27. Zhang, H.; Cao, G. P.; Wang, Z. Y.; Yang, Y. S.; Shi, Z. J.; Gu, Z. N. *Nano Lett.* **2008**, *8*, 2664.
28. Meng, C. Z.; Liu, C. H.; Fan, S. S. *Electrochem. Commun.* **2009**, *11*, 186.
29. Lee, H.; Cho, M. S.; Kim, I. H.; Nam, J. D.; Lee, Y. K. *Synth. Met.* **2010**, *160*, 1055.
30. Biswas, S.; Drzal, L. T. *Chem. Mater.* **2010**, *22*, 5667.
31. Sun, X. F.; Xu, Y. L.; Wang, J.; Mao, S. C. *Int. J. Electrochem. Sci.* **2012**, *7*, 3205.
32. Mi, H. Y.; Zhang, X. G.; Xu, Y. L.; Xiao, F. *Appl. Surf. Sci.* **2010**, *256*, 2284.
33. Ham, H. T.; Choi, Y. S.; Jeong, N.; Chung, I. *J. Polymer* **2005**, *46*, 6308.
34. Sun, Y. G.; Rogers, J. A. *Adv. Mater.* **2007**, *19*, 1897.
35. Kaltenbrunner, M.; Kettlgruber, G.; Siket, C.; Schwödiauer, R.; Bauer, S. *Adv. Mater.* **2010**, *22*, 2065.
36. Hu, L. B.; Pasta, M.; Mantia, F. L.; Cui, L. F.; Jeong, S.; Deshazer, H. D.; Choi, J. W.; Han, S. M.; Cui, Y. *Nano Lett.* **2010**, *10*, 708.
37. Kaltenbrunner, M.; White, M. S.; Glowacki, E. D.; Sekitani, T.; Someya, T.; Sariciftci, N. S.; Bauer, S. *Nat. Commun.* **2012**, *3*, 770.
38. Hiralal, P.; Imaizumi, S.; Unalan, H. E.; Matsumoto, H.; Minagawa, M.; Rouvala, M.; Tanioka, A.; Amaratunga, G. A. *J. ACS Nano* **2010**, *4*, 2730.
39. Nam, K. T.; Kim, D. W.; Yoo, P. J.; Chiang, C. Y.; Meethong, N.; Hammond, P. T.; Chiang, Y. M.; Belcher, A. M. *Science* **2006**, *312*, 885.
40. Chen, J.; Liu, Y.; Minett, A. I.; Lynam, C.; Wang, J. Z.; Wallace, G. G. *Chem. Mater.* **2007**, *19*, 3595.
41. Wang, H. J.; Peng, C.; Peng, F.; Yu, H.; Yang, *J. Mater. Sci. Eng. B* **2011**, *176*, 1073.
42. Frackowiak, E.; Khomenko, V.; Jurewicz, K.; Lota, K.; Beguin, F. *J. Power Sources* **2006**, *153*, 413.
43. Luo, Z. H.; Zhu, L. H.; Huang, Y. F.; Tang, H. *Synth. Met.* **2013**, *175*, 88.
44. Yu, G. H.; Hu, L. B.; Vosgueritchian, M.; Wang, H. L.; Xie, X.; McDonough J. R.; Cui, X.; Cui, Y.; Bao, Z. N. *Nano Lett.* **2011**, *11*, 2905.
45. Chen, W.; Rakhi, R. B.; Hu, L. B.; Xie, X.; Cui, Y.; Alshareef, H. N. *Nano Lett.* **2011**, *11*, 5165.
46. Liu, F. F.; Han, G. Y.; Chang Y. Z.; Fu, D. Y.; Li, Y. P.; Li, M. Y. *J. Appl. Polym. Sci.* **2014**, *131*, 39779.
47. Jin, M.; Han, G. Y.; Chang, Y. Z.; Zhao, H.; Zhang, H. Y. *Electrochim. Acta* **2011**, *56*, 9838.
48. Han, G. Y.; Yuan, J. Y.; Shi, G. Q.; Wei, F. *Thin Solid Films* **2005**, *474*, 64.

49. Xu, Y. X.; Zhao, L.; Bai, H.; Hong, W. J.; Shi, G. Q. *J. Am. Chem. Soc.* **2009**, *131*, 13490.

50. Fan, Z. J.; Yan, J.; Wei, T.; Zhi, L. J.; Ning, G. Q.; Li, T. Y.; Wei, F. *Adv. Funct. Mater.* **2011**, *21*, 2366.

51. Zhang, L.; Shi, G. Q. *J. Phys. Chem. C* **2011**, *115*, 17206.

52. Li, S.; Wang, L.; Tian, C. G.; Xie, Y.; Shi, K. Y.; Li, M. T.; Fu, H. G. *RSC Adv.* **2012**, *2*, 4498.

53. Zhang, L. L.; Zhao, X.; Stoller, M. D.; Zhu, Y. W.; Ji, H. X.; Murali, S.; Wu, Y. P.; Perales, S.; Clevenger, B.; Ruoff, R. S. *Nano Lett.* **2012**, *12*, 1806.

54. Bobacka, J.; Lewenstam, A.; Ivaska, A. *J. Electroanal. Chem.* **2000**, *498*, 17.

55. Ardizzone, S.; Fregonara, G.; Trasatti, S. *Electrochem. Acta* **1990**, *35*, 263.